Variable Camshaft Timing Engine Control

A. G. Stefanopoulou, J. S. Freudenberg, J. W. Grizzle

Abstract— **Retarding camshaft timing in an engine equipped with a dual equal camshaft timing phaser reduces the unburned hydrocarbons (HC) and oxides of nitrogen (NO_x) emitted to the exhaust system. Apart from this positive effect to feedgas emissions, camshaft timing can cause large air-to-fuel ratio excursions if not coordinated with the fuel command. Large air-to-fuel ratio excursions can reduce the catalytic converter efficiency and effectively cancel the benefits of camshaft timing. The interaction between the camshaft timing and the air-to-fuel ratio results in an inherent tradeoff between reducing feedgas emissions and maintaining high catalytic converter efficiency. By designing and analyzing a decentralized and a multivariable controller, we describe the design limitation associated with the decentralized controller architecture and we demonstrate the mechanism by which the multivariable controller alleviates the limitation.**

Keywords— **Multivariable Feedback Control, Air-to-Fuel Ratio, Emissions, Pollution Control, Internal Combustion Engines.**

I. Introduction

Optimization and real-time control of cam timing in an engine equipped with a dual equal camshaft timing phaser can potentially reduce the unburned hydrocarbons (HC) and oxides of nitrogen (NO_x) emitted to the exhaust system ([20], [12]). In particular, by retarding the cam timing, combustion products which would otherwise be expelled during the exhaust stroke are retained in the cylinder during the subsequent intake stroke. The contribution of this diluent to the mixture in the cylinder reduces the HC and NO_x feedgas emissions. On the other hand, the diluent affects the fresh air mass charge into the cylinders, thus altering the torque response and acting as a disturbance in the A/F loop. The effect of cam timing to torque response is undesirable due to potential drivability issues. Moreover, the effect of cam timing on A/F is undesirable due to potential degradation of catalytic converter efficiency. A mathematical model of an experimental engine equipped with a variable cam timing mechanism (VCT) has been derived in [17]. The VCT engine was shown to have very strong interactions among the cam timing (CAM), the air-to-fuel ratio (A/F), and the torque (T_q) response.

In this paper we design a model-based controller that coordinates variable camshaft timing and fuel charge in an internal combustion engine to reduce feedgas emissions, regulate air-to-fuel ratio (A/F) at stoichiometry, and maintain torque response similar to that of a conventional (fixed cam timing) engine.

Despite the various studies of variable valve schemes ([3], [5], [9], [10], [12], [20], and references therein) there is no systematic investigation of a control scheme which can achieve improved overall engine performance. The difficulties lie in three areas: (i) the performance objectives are interrelated and impose severe tradeoffs in the control design, (ii) measurements of the performance variables are unavailable or largely delayed due to cost or technological limitations, and (iii) implementation and calibration favor decentralized controller architectures that constrain controller design. These three difficulties exist in many industrial control applications and there are no well accepted guidelines that will ensure a satisfactory solution. For the variable cam timing engine, issue (i) arises from the fact that minimization of feedgas emissions, smooth engine torque response, and tight A/F regulation at stoichiometry are conflicting objectives due to their subsystem interactions. Issue (ii) arises because real-time measurements of torque and feedgas emissions are not currently available in conventional vehicles. Furthermore, A/F measurement is largely delayed imposing bandwidth limitations in the feedback loop.

Issues (i) and (ii) are currently addressed only in steady-state using off-line optimization of static engine mapping data. The control problem is usually defined as a tracking problem with set-points provided by steady-state optimization. The feedback control problem is to track the steady-state cam command with a specified speed of response and regulate A/F at stoichiometry. Conventional feedback control design practice in the automotive industry is to calibrate multiple single-input singe-output control loops to achieve individual subsystem performance. Such an approach results in decentralized controller development satisfying the third requirement above (issue (iii)). On one hand, this approach allows efficient organization of the engineering task of implementation. On the other hand, this approach often results in less than optimal system performance, especially when, the overall system is calibrated by de-tuning a subsystem controller to avoid unintentional excitation of another subsystem. The design of decentralized controllers can potentially impose a large calibration burden in time and effort for highly coupled systems such as the VCT engine [2].

In this paper we concentrate on the interactions between the cam timing and the A/F response. This interaction results in an inherent tradeoff between reduc-

Work was supported by the National Science Foundation under contract ECS-96-31237 (Grizzle), ECS-94-14822 (Freudenberg), and ECS-97-33293 (Stefanopoulou); matching funds to these grants were provided by Ford Motor Co.

A. G. Stefanopoulou is with the Mechanical and Environmental Engineering Department, University of California, Santa Barbara

J. S. Freudenberg and J. W. Grizzle are with the Control Systems Laboratory, Department of Electrical Engineering and Computer Science, University of Michigan

ing feedgas emissions and maintaining high catalytic converter efficiency. By designing and analyzing a decentralized and a multivariable linear controller, we describe the design limitation associated with the decentralized controller architecture and we demonstrate the mechanisms by which the multivariable controller alleviates the limitation. We finally simplify the fully multivariable controller to a lower triangular form with equivalent closed-loop performance. The results are based on linear analysis of the subsystem interactions at one operating point and evaluated using a nonlinear simulation model. This type of analysis is valuable because it indicates that a multivariable controller, at least at this operating point, gives performance enhancements.

Several other simplifications of the VCT engine control problem are employed. We do not consider external exhaust gas recirculation (EGR) because variable cam timing increases the internal exhaust gas recirculation (dilution) and can potentially eliminate the need for external EGR. Spark timing is assumed to be scheduled at minimum spark advance to achieve best torque (MBT). We also ignore the effects of the cam timing on the characteristics of backflow and temperature of the surface where the fuel is injected. In general, variable camshaft timing allows operation at higher intake manifold pressures, reduces the backflow through the intake valve and can consequently reduce the uncertainty in the fuel evaporation rate. Our inability to measure (or robustly infer from other measurements) torque and feedgas emissions limits us to "off-line" design of the cam timing loop bandwidth. We define the cam timing bandwidth that achieves a reasonable tradeoff between torque performance and averaged feedgas emissions. The problem of transient torque control for an engine equipped with VCT is addressed in [19]. The potential of using additional actuators such as drive-by-wire throttle or an air-bypass valve in torque management of a VCT engine is investigated in [7], [8].

This paper is organized as follows. Nomenclature is defined in Section II. In Section III, we formulate the VCT engine control problem. The performance tradeoff between torque performance and feedgas emissions is described in Section IV. This tradeoff leads to the derivation of the static cam timing schedule, Section IV-A, and the bandwidth of the cam timing loop, Section IV-B. The cam timing and A/F feedback control design are derived in Section V. The A/F controller consists of a feedforward fuel command that depends on an air charge estimation which is described in Section VI; and a feedback fuel command that depends upon a linear exhaust gas oxygen sensor (UEGO) which is described in Section VII. In Sections VII-A and VII-B we show that by allowing the fuel command to depend on cam timing we achieve tighter A/F control at the expense of more complex controller architecture. The VCT engine controller design is evaluated using a simulation of the nonlinear VCT engine model; simulations results are shown in Section VIII. Finally, our conclusions are summarized in Section IX.

II. Nomenclature

A/F	air-to-fuel ratio A/F_{cyl} : air-to-fuel ratio in the cylinder A/F_{exh} : air-to-fuel ratio at the UEGO sensor A/F_{stoic} : stoichiometric air-to-fuel ratio
c	coefficients on physical equations (with various subscripts) controller terms command when used in subscripts
CAM	camshaft timing (degrees) CAM_c : commanded camshaft timing CAM_a : actual camshaft timing CAM_m : measured camshaft timing CAM_{des} : desired camshaft timing
F_c	fuel command (gr/event)
fw	feedforward (as an index)
fb	feedback (as an index)
K, or k	static gains derived after linearization
$\dot{m}$	mass air flow rate (gr/s) $\dot{m}_\theta$: mass air flow rate through the throttle body $\dot{m}_{cyl}$: mass air flow rate to the cylinder
m	mass (gr) m_a : mass air charge (gr/event)
MAF	mass air flow measured using a hot wire anemometer
N	engine speed (rpm)
P	pressure (bar) P_m : manifold pressure (bar) P_o : atmospheric pressure (bar)
R	specific gas constant (J/KgK)
T	temperature or torque (it is made clear through the context)
V_m	manifold volume (m^3)
ΔT	fundamental sampling time interval (s)
θ	throttle angle (degrees)
τ	time constant in lowpass filters (s)

III. Overview of the Controller Architecture

In this section we formulate the control problem. During rapid throttle changes imposed by the driver we need to control cam timing and fuel charge to regulate A/F at stoichiometry and minimize feedgas NO_x and HC emissions, under the constraint of monotonic brake torque response. Feedgas emissions and torque response cannot be used as feedback signals because they are not currently measured in the vehicle (stringent emission standards might require the introduction of such sensors in the future). Figure 1 shows the input and output signals of the VCT engine as they are used in the control design. The control problem at hand, shown in Figure 1, has three performance variables (we can lump NO_x and HC in one variable) and two control variables.

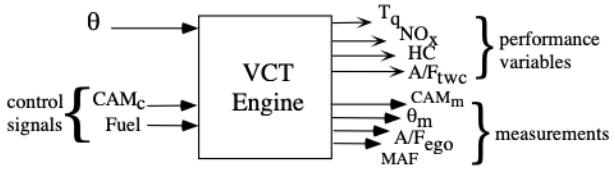

Fig. 1. Input-output relationship for the VCT engine control problem.

Cam timing is primarily used to reduce the feedgas emissions. Although dynamic measurements of feedgas

emissions are not available, there is a simple rule to follow: "retarded cam timing reduces feedgas emissions" [17]. We cannot, however, operate always in retarded cam because retarded cam timing affects the dilution in the cylinders, which in turn alters the torque response. Therefore the cam timing loop must satisfy a reasonable tradeoff between reducing feedgas emissions and maintaining monotonic torque response. We design the steady-state cam timing schedule based on throttle angle measurement. The resulting static cam timing schedule allows operation in maximum retarded cam when combustion stability and adequate torque can be achieved. Based on this static cam timing schedule, we define a tracking problem for the cam timing loop. The bandwidth of the cam timing loop is determined off-line to avoid undesirable excitation to transient torque response. Detailed analysis and design of the cam timing loop bandwidth can be found in [19].

The bandwidth in the A/F feedback loop is determined by the delay associated with the A/F measurement at a linear exhaust gas oxygen (UEGO) sensor, A/F_{exh} signal. Throttle and cam timing alter the air charge and therefore act as a disturbance in the A/F loop. The fuel command cannot reject this disturbance based on the delayed A/F_{exh} signal, so a two degree of freedom A/F controller will be used.

The resulting controller structure, shown in Figure 2, consists of a steady-state cam timing schedule, a feedforward fuel controller and a multiple-input multiple-output (MIMO) feedback controller. During throttle changes, the feedback controller will be tracking cam timing to the desired cam timing position, and maintain A/F at stoichiometry. The interaction between the cam timing and A/F loops suggests the development of a fully multivariable feedback controller. On the other hand, two PI feedback loops (decentralized controller) would ensure independent development of the new feature, cam timing. Here, the motivation arises from the fact that if the simpler controller structure results in satisfactory performance, then addition of the variable cam timing mechanism to a conventional automotive engine does not require completely new software development and calibration procedures, but merely involves calibration of (i) the PI gains in the A/F loop and (ii) the bandwidth of the cam phasing dynamics (see Figure 3).

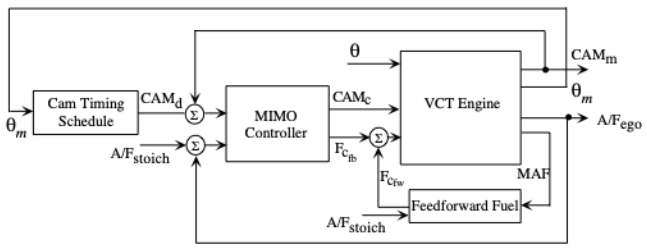

Fig. 2. Overview of the MIMO controller structure.

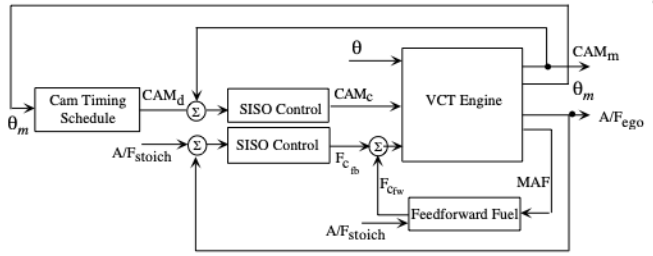

Fig. 3. Controller structure when cam timing and A/F control are two separate SISO controllers.

IV. Torque Requirements

The control requirement is to maintain brake torque response similar to the conventional engine at constant engine speed during rapid throttle changes. Engine speed is a slowly varying parameter and can be assumed constant for rapid changes in throttle position imposed by the driver during rapid acceleration demands. Simulations showed that varying engine speed provides a dampening factor in the engine power response. Hence, imposing constraints upon the engine torque response is a conservative way of addressing drivability requirements.

In the next two sections we briefly describe the design specifications for the cam timing loop. The static feedforward cam timing schedule is determined based on its effect on the steady-state torque response; the bandwidth of the cam timing loop is determined based on its effect on the transient torque response.

A. Feedforward Cam Timing Schedule

The static cam timing schedule is designed off-line based on the static effects of cam timing on engine torque response. Figure 4 (left) shows the torque response for a conventional cam timing ($CAM = 0$ degrees—dashed line) and maximum retarded cam timing ($CAM = 35$ degrees—dashed-dot line) versus throttle angle at 2000 RPM. To minimize feedgas emissions we need to operate at maximum cam retard. To ensure maximum torque at wide open throttle (WOT) we need to advance cam timing back to the base cam timing. The solid line in Figure 4 (left) shows a smooth transition from fully retarded to base cam timing for part throttle to WOT. For very small throttle angles (low load), cam timing does not affect the static torque response[1], but it deteriorates the combustion stability because of the high level of dilution.

Cam timing, therefore, is scheduled at base cam timing for small throttle angles to avoid increase of unburned HC and to maintain combustion stability. Hence, the steady-state cam phasing, $CAM_{des} = G(\theta_m, N_m)$, that minimizes feedgas emissions while maintaining smooth steady-state torque response is scheduled as follows: (1) near idle it

[1]Cam timing does not affect the steady-state flow through the throttle body during sonic conditions. Detailed discussion of the nonlinear engine behavior due to the two distinct regimes of flow through the throttle body can be found in [18].

is scheduled for idle stability which requires cam phasing equal to zero; (2) at mid-throttle it is scheduled for emissions which favors fully retarded cam phasing; and (3) at wide open throttle (WOT) it is scheduled for maximum torque which requires cam phasing to be advanced back to 0 degrees. The developed cam scheduling scheme, shown in Fig. 4 (right), ensures reduction of feedgas emissions under the constraint of smooth steady state torque response for constant engine speed.

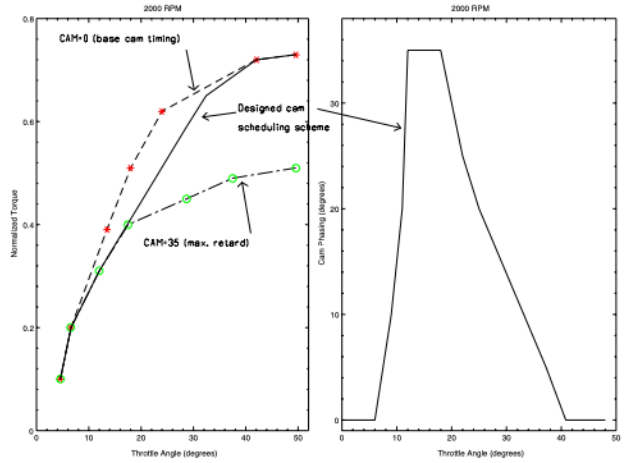

Fig. 4. Comparison between static torque response using the conventional cam phasing ($CAM = 0$ degrees), the designed cam scheduling scheme, and the fully retarded cam phasing. The designed cam scheduling scheme is shown in the right figure.

B. Transient Cam Timing

The speed of cam timing changes during throttle steps can dramatically affect the brake torque response and even cause undershoot during throttle tip-in. This behavior is consistent with the results in [16], where it is shown that the torque response of the VCT engine during coordinated throttle and cam steps can be described by a non-minimum phase system. It is known that the undershoot in a system with a non-minimum phase zero will increase if we require a short settling time, and thus fast speed of response (pp. 15, [15]). Therefore, reduction of the feedgas emissions and good dynamic torque response cannot be achieved independently: good torque response favors slow cam phasing to the new set points, but this might degrade the feedgas emissions which require fast cam transients. The following simulations illustrate a compromise between the torque response and emissions, and will be used to define the cam phasing control loop bandwidth.

Figure 5 illustrates cam phasing and torque response to step changes in throttle position at 750, and 2000 rpm (left and right plots respectively). In all simulations, stoichiometric A/F and MBT spark timing were used. Therefore the torque response in Fig. 5 is only a function of air charge and internal exhaust gas recirculation (or cam phasing). For simplicity, the closed-loop cam phasing dynamics are described by a low-pass filter between the desired and the commanded cam phasing. Figure 5 shows the cam phasing and torque response in closed loop with time constants of 0.5, 1.0 and 1.5 engine cycles. Good torque response is a critical requirement at low engine speeds, and a time constant of 1 engine cycle was considered sufficient for 750 RPM. At 2000 rpm the interaction between torque and cam phasing loop is considerably weaker than the interaction at lower engine speeds, and a time constant of 1 engine cycle is once again adequate for the cam phasing controller. Thus, the bandwidth of the cam phasing controller is scheduled in this paper as a function of engine speed to correspond to 1 engine cycle in order to achieve a reasonable torque response over the entire operating regime. An extended analysis of the selection of the optimal cam phasing time constant as a function of throttle position and engine speed can be found in [19].

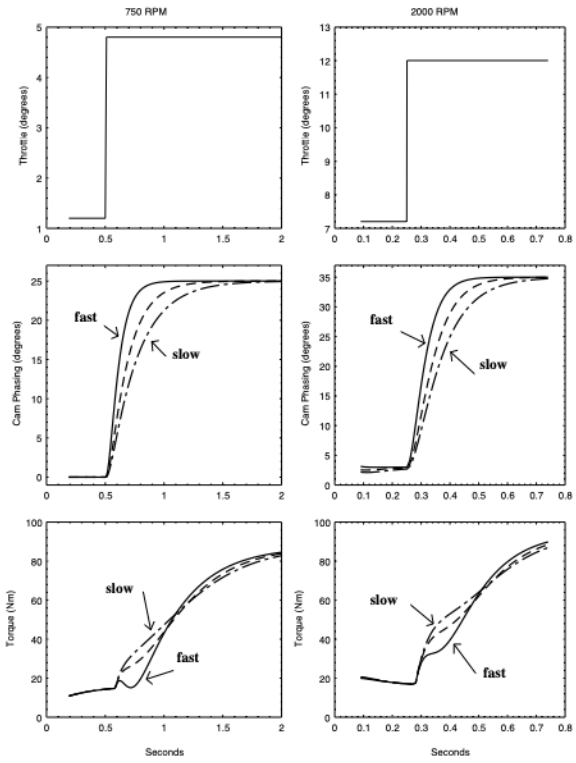

Fig. 5. Torque response (at 750 and 2000 RPM) using different low-pass filters in the cam phasing dynamics.

V. Emissions Requirements

In the VCT engine, changes in the throttle position are followed by changes in the cam phasing based on the scheduling scheme shown in Fig. 4. The desired cam phasing reduces feedgas emissions by regulating the diluent in the cylinders. The contribution of this diluent to the mixture in the cylinder affects the breathing process, and consequently the mass charge in the cylinders, which in turn affects the air fuel ratio (A/F) in the cylinder mixture. This makes the A/F response highly coupled with the cam phasing activity. Cam phasing is used to regu-

late feedgas emissions during changes in throttle position, but through its interaction with A/F, it also affects the catalytic converter efficiency.

We will achieve reduction of tailpipe emissions if we reduce feedgas emissions at equivalent catalytic converter efficiency. Therefore, to improve feedgas emissions we need to regulate cam timing to its steady-state value as fast as possible while maintaining A/F at stoichiometry. Unfortunately the long delay (810 degrees) in the A/F measurement associated with the combustion-exhaust stroke and the transport delay in the exhaust manifold imposes a bandwidth limitation on the A/F loop. If the disturbance to the A/F loop caused by the cam activity has high frequency content (i.e., beyond the achievable bandwidth of the A/F controller), then the disturbance cannot be rejected. In this case, it is a common technique to slow down the cam phasing signal, i.e., to de-tune the subsystem that causes the high frequency disturbance. This alternative, although consistent with current design practice, entails loss of the potential emissions benefits of the VCT engine.

Hence, the dynamic performance tradeoff is between (a) the feedgas emissions that the catalytic converter must process and (b) the efficiency of the catalytic converter (which is a function of A/F excursions from stoichiometry). Due to the interaction between the cam timing loop and the A/F loop, we cannot simultaneously minimize (a) and maximize (b); this is because maximum catalytic efficiency requires that A/F be held perfectly at stoichiometry, which in turn rules out moving the cam rapidly to reduce feedgas emissions. A dynamic model of the catalytic converter efficiency could help specify a rigorous tradeoff between the two bandwidths, because, after all, the ultimate goal is to minimize tailpipe emissions [1]. Here, for simplicity we selected the bandwidth of the cam phasing loop that satisfies the torque requirements, one engine cycle (720 degrees).

To achieve good A/F control during rapid throttle and cam movements we utilize the commonly used two degree of freedom A/F controller topology modified for the variable cam timing engine [6]. The A/F control loop consists of a feedforward term that adjusts the fuel command based on the measured mass air flow (MAF) and the measured cam position (CAM_m), and a feedback term that regulates the fuel command based on the significantly delayed A/F signal from the EGO sensor.

VI. Feedforward Design

The feedforward term is based on the estimation of the cylinder pumping mass air flow rate ($\widehat{\dot{m}_{cyl}}$) from the measured cam phasing (CAM_m), the estimated manifold pressure ($\widehat{P_m}$), and the engine speed

$$\widehat{\dot{m}_{cyl}} = P(CAM_m, \widehat{P_m}, N) \tag{1}$$

The estimated manifold pressure ($\widehat{P_m}$) is calculated as:

$$\frac{d}{dt}\widehat{P_m} = K_m(\tau\frac{d}{dt}MAF + MAF - \widehat{\dot{m}_{cyl}}) \tag{2}$$

where we have used the dynamics of the mass air flow meter : $\tau\frac{d}{dt}MAF + MAF = \dot{m}_\theta$. To eliminate the derivative on the air flow measurement, we use the variable $\chi = \widehat{P_m} - K_m \cdot \tau \cdot MAF$. This yields the estimated cylinder mass air flow rate :

$$\begin{aligned} \tfrac{d}{dt}\chi &= K_m(MAF - \widehat{\dot{m}_{cyl}}) \\ \widehat{P_m} &= \chi + K_m \cdot \tau \cdot MAF \\ \widehat{\dot{m}_{cyl}} &= P(CAM_m, \widehat{P_m}, N) \end{aligned} \tag{3}$$

For the estimation of the mass air charge into the cylinders ($\widehat{m_a}$), we assumed uniform flow during the fundamental engine event ($\Delta T = \frac{120}{n \cdot N}$, where n, the number of cylinders equals 8, and N is the engine speed in rpm):

$$\widehat{m_a} = \widehat{\dot{m}_{cyl}} \cdot \Delta T = \widehat{\dot{m}_{cyl}} \cdot \frac{15}{N} \tag{4}$$

The feedforward fuel command is given by $F_{c_{fw}} = \frac{\widehat{m_a}}{14.64}$.

VII. Feedback Design

In this section we design a linear feedback controller that tracks the desired cam timing as defined by the static cam scheduling scheme, and maintains A/F at stoichiometry (see Fig. 2). The controller design considerations are: (a) There is an 810 degree delay in the A/F process. At 2000 rpm, this translates into a time delay of 0.0675 sec. The A/F bandwidth should not exceed 7.5 rad/sec since by using a Padé approximation for the 0.0675 sec delay we have the deleterious effects of a non-minimum-phase zero approximately at 15 rad/sec. (b) The required time constant for the cam phasing dynamics is 720 degrees (1 engine cycle). At 2000 rpm this corresponds to a time constant equal to 0.06 sec, which translates into a cam phasing closed-loop bandwidth equal to 17 rad/sec.

We linearized the model at a throttle position equal to 9.33 degrees, cam phasing equal to 10 degrees, and engine speed equal to 2000 rpm. This operating point lies in the transition region on the cam phasing scheduling scheme shown in Fig. 4. The delays are represented by 1st and 2nd order Padé approximations. The linear model has 9 states and 2 integrator states are introduced to ensure zero steady-state error in tracking the desired cam timing and the stoichiometric A/F. Figure 6 shows the Bode gain plots of the plant linearized at 2000 RPM. Cam phasing is measured in degrees, A/F is dimensionless, and the fuel command is scaled so that a unit deviation in fuel causes a unit deviation in the A/F signal. The plant has a lower triangular form, i.e., there is no interaction between the fuel command and the cam phasing loop, since fuel charge affects the system downstream of the breathing process.

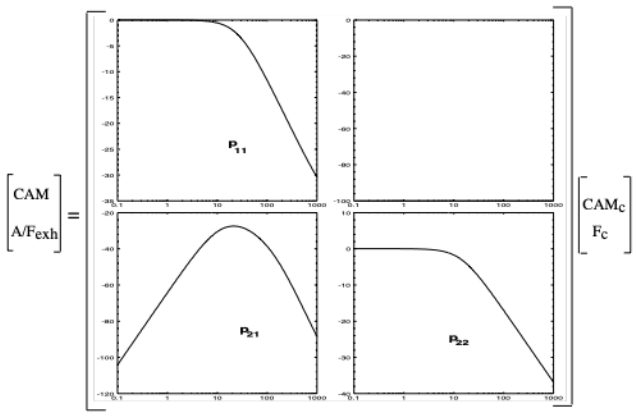

Fig. 6. Bode gain plots of the linearized plant.

In Figure 6 we can see the interaction term (p_{21}) between the cam phasing control signal and A/F measurement. The feedforward portion of the A/F controler described in Section VI ensures decoupling of the cam phasing and the A/F in steady-state, but allows high frequency interaction. The peak of the interaction term occurs at 20 rad/sec while we require the cam phasing activity to roll off after 17 rad/sec. Therefore, the control signal generated to force the cam phasing to track a command input will also produce a transient response in the A/F loop; in effect, the cam loop acts as a disturbance to the A/F loop. Furthermore, there is a $9\Delta T$ sec delay (shown in Fig. 7) that is located downstream of the disturbance from the cam loop to the the A/F loop. We thus see that we have a two-input two-output (TITO) system with strong interaction between the two loops and a bandwidth limitation due to the sensor delay.

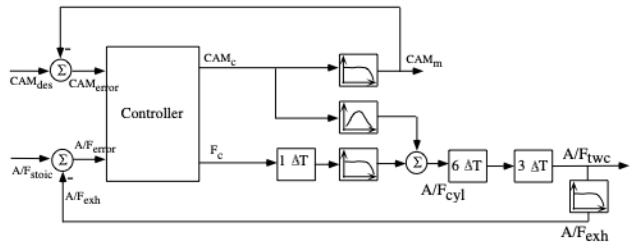

Fig. 7. Block diagram of the linearized plant.

The simplest approach to design the feedback controller is to ignore the interaction between the two loops and design two SISO feedback systems (see Fig 3). It is well known, however, that multivariable controllers manage design tradeoffs due to subsystem interactions more successfully than do decentralized controllers [13], [4]. In [11] it is mentioned that multivariable design techniques reduce the interaction between subsystems even without having taken explicit steps to do so. For this reason in the following subsections we design a multivariable and a decentralized controller and study their impact on the emissions performance.

A. TITO and 2 SISO Design

A multivariable controller was designed to track the desired cam phasing as described in Sec. IV-A and maintain A/F at stoichiometry. The controller schedules the fuel and cam phasing commands based on the cam phasing position measurement and the A/F signal from the EGO sensor. The LQG/LTR methodology was used because it provided a straightforward way to meet the performance requirements discussed in Sec. VII, and has been studied extensively for its robustness properties [11]. Robustness issues in VCT design arise because the VCT engine model used for design does not include fuel puddling dynamics which is considered as input uncertainty in the fuel path. Also, there is a significant uncertainty in the cam phaser dynamics due to aging. A comprehensive study of robustness requires more extensive modelling of these and other uncertainties and is beyond the scope of the present paper.

A few design iterations yielded the decentralized and the multivariable controllers, the Bode gain plots of which are illustrated in Figure 8. Appendices B and C contain detailed description of the two controllers. Both controller designs achieve the bandwidth requirement in the cam phasing loop, and provide adequate speed of response in the A/F loop.

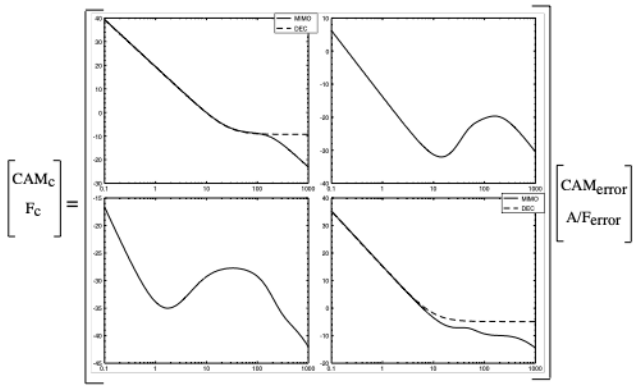

Fig. 8. Bode gain plots of the two controllers.

Note that the diagonal elements of the two controllers are approximately identical. The reason for this will become clear in the next section, where we see that the bandwidth specifications for the two loops essentially fix the bandwidths of the diagonal elements of the controller, independently of the controller structure.

Comparisons between the system response with the previously selected diagonal controller (see Figure 8), and the system response with a decentralized controller consisting of the diagonal elements of the multivariable controller, showed only negligible differences. Hence, for the rest of this study, we will simply compare and discuss the decentralized controller obtained by using the diagonal elements of the multivariable controller and the fully multivariable controller.

Figure 9 shows linear simulations of the output and control signals during various cam phasing step commands for

the two different controller architectures. The A/F deviations for the multivariable control scheme are significantly better than those corresponding to the decentralized control scheme. Implementing the multivariable controller thus seems to be beneficial. The questions we must address are: How did the multivariable controller manage to reject the A/F disturbance faster than the decentralized controller? In which way did the multivariable controller reduce the interaction between the two loops? In the next section we identify the mechanism by which the multivariable controller achieves smaller A/F excursions during cam phasing transients.

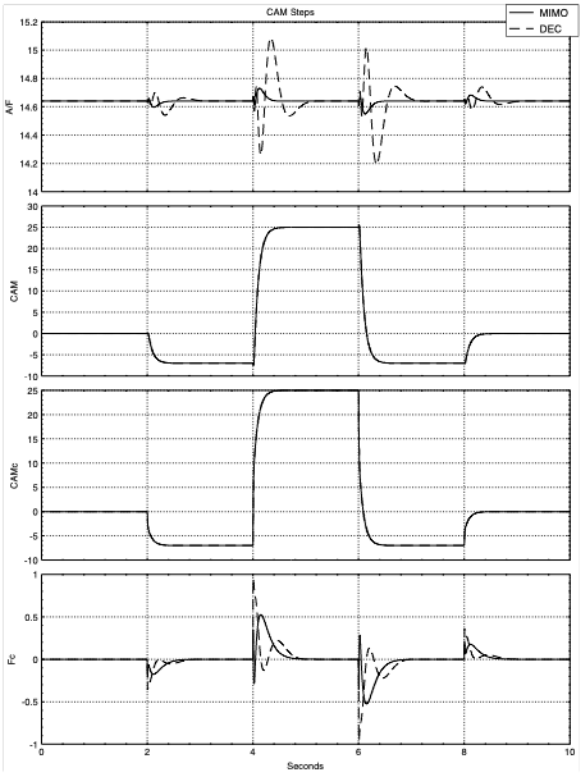

Fig. 9. Linear simulation during cam phasing commands.

B. TITO and 2 SISO Analysis

We begin by describing a design limitation present with decentralized control. Consider the decentralized control system in Figure 10. Topologically, the CAM loop acts as an output disturbance to the A/F loop. As noted in Section V, there is no interaction from the A/F loop to the CAM loop.

Denote the sensitivity and complementary sensitivity functions for each loop by $s_{ii}(s) = (1+p_{ii}(s)c_{ii}(s))^{-1}$ and $t_{ii}(s) = 1 - s_{ii}(s)$, $i = 1, 2$. Then the transfer function describing the closed-loop A/F response is given by

$$\begin{aligned} A/F_{exh}(s) &= t_{22}(s)A/F_{stoic}(s) \\ &+ s_{22}(s)p_{21}(s)\underbrace{c_{11}(s)s_{11}(s)CAM_{des}(s)}. \end{aligned} \tag{5}$$

The term underlined in (5) is equal to $CAM_c(s)$, the control signal in the CAM loop generated in response to a CAM command (CAM_{des}). As we have seen, the plant interaction (quantified by the transfer function $p_{21}(s)$), causes this signal to act as a disturbance to the A/F loop.

Suppose that this closed-loop interaction results in unacceptable A/F transients. With a decentralized controller structure, there are two alternate approaches to reducing the interaction:

(i) Increase the bandwidth of the A/F loop, thus obtaining smaller sensitivity ($\mid s_{22}(j\omega) \mid \ll 1$), and greater disturbance attenuation, over a wider frequency range. This alternative is not feasible in the present problem, because the time delay limits the speed of response in the A/F loop.

(ii) Decrease the bandwidth of the CAM loop to obtain less control activity ($\mid c_{11}(j\omega)s_{11}(j\omega) \mid \ll 1$) at the frequencies of the problematic interaction. This alternative has been ruled out because it entails loss of potential benefits of the variable cam timing engine, as argued in Section V.

The preceding analysis implies the existence of a tradeoff between CAM and A/F responses. Specifically, to reduce the undesirable effects of interaction from CAM command to A/F response, it is necessary to either reduce the bandwidth in the CAM loop, and/or increase the bandwidth in the A/F loop. Increasing the speed of the A/F response is not feasible due to the time delay; hence, the tradeoff is resolved by sacrificing CAM performance in favor of the A/F loop.

We have seen that a decentralized controller structure imposes a tradeoff between achieving the bandwidth specifications in the two loops. Let us now consider two mechanisms by which a MIMO controller can (potentially) mitigate such a tradeoff.

(1) Let the CAM control signal depend upon errors in both cam and A/F loops (the term (c_{12}) in Figure 11). Essentially, this strategy allows the controller for the CAM loop to achieve a compromise between regulating errors in the two loops and is an elegant alternative to the de-tuning practice, (ii), that we mentioned above. In the present case, this method is not useful because the delay occurs after the disturbance, and thus the disturbance is measured too late to allow either actuator to compensate for it. The significantly delayed A/F measurement cannot contribute information through the term (c_{12}) sufficient rapidly to slow the cam activity. Indeed, in Figure 9 we can observe the nearly identical cam phasing control signals issued by the two controllers. We verified that the MIMO controller does not make effective use of the A/F error in computing the CAM control signal by zeroing the term (c_{12}) of the MIMO controller and noting that closed-loop performance is virtually unchanged.

(2) Let the fuel signal depend upon the error in both CAM and A/F loops (the term (c_{21}) in Figure 11). As depicted in Figure 12, this control strategy results in a

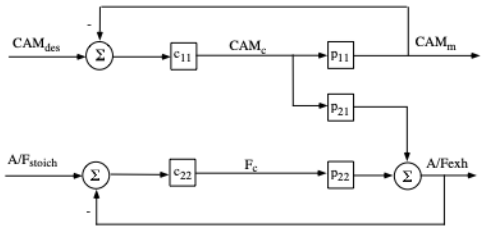

Fig. 10. Block diagram of the decentralized control scheme.

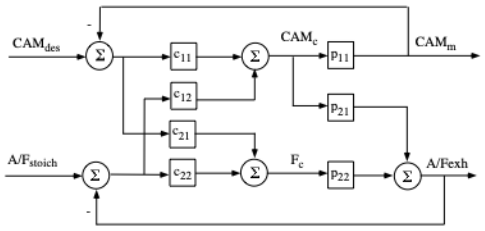

Fig. 11. Block diagram of the fully multivariable scheme.

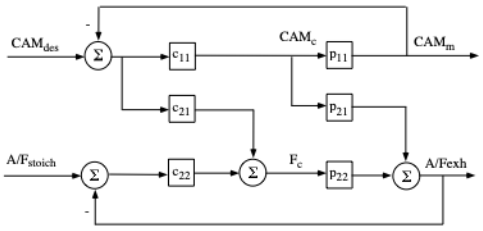

Fig. 12. Block diagram of the simplified multivariable control scheme.

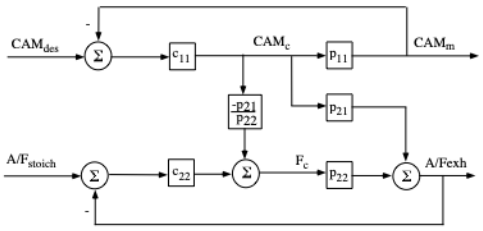

Fig. 13. Block diagram of the decoupling controller.

feedforward path from the cam phasing error to the fuel command used to control A/F. The feedforward term (c_{21}) sends information to the fuel command about the cam phasing error, and this allows faster response during cam phasing transients. The disturbance imposed on the A/F loop by a command issued to the cam phasing loop is shown in the following equation :

$$A/F_{exh}(s) = (p_{21}(s)c_{11}(s) + p_{22}(s)c_{21}(s))CAM_{error}(s) \tag{6}$$

Note here, that the same disturbance for the decentralized controller (see Figure 10) is given by :

$$A/F_{exh} = p_{21}(s)c_{11}(s)CAM_{error}(s) \tag{7}$$

The multivariable controller can potentially reduce the coupling between the two subsystems by choosing the term (c_{21}) such that

$$\mid p_{21}(j\omega)c_{11}(j\omega) + p_{22}(j\omega)c_{21}(j\omega) \mid < \mid p_{21}(j\omega)c_{11}(j\omega) \mid \tag{8}$$

It is possible to interpret the action of the MIMO controller as partially decoupling the A/F response from the CAM loop. Indeed, setting the feedforward term equal to

$$c_{21}(s) = \frac{-c_{11}(s)p_{21}(s)}{p_{22}(s)} \tag{9}$$

achieves zero closed-loop interaction from CAM to A/F. An alternate representation of the perfect decoupler (9) is depicted in Figure 13. With this topology, the CAM and A/F loops become completely decoupled, and the two remaining controller parameters, c_{11} and c_{22}, may be chosen independently. This controller design may be prone to robustness problems, since the term (c_{21}) is canceling the undesired disturbance by inverting the signal along the path of the plant interaction.

In practice, there is no need to achieve perfect decoupling. In Figure 14, we see that MIMO control reduces only the peak in the closed-loop response from CAM commands to A/F measurements. Indeed, at lower frequencies, the integral action in the A/F loop achieves zero steady state error despite the interaction with the CAM loop. At higher frequencies, on the other hand, the CAM loop rolls off and thus does not produce a response in A/F. As we see in Figure 14, the MIMO controller merely reduces the peak due to the interaction, thus attenuating the effect of the CAM loop upon A/F without achieving total decoupling.

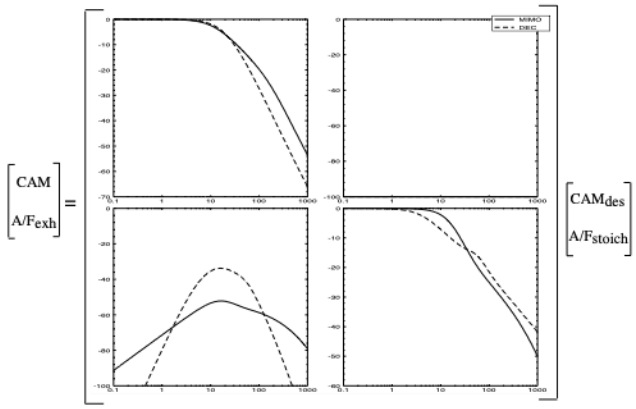

Fig. 14. Bode gain plots of the closed-loop transfer function.

Nevertheless, the feedforward term (c_{21}) depends upon the plant model and the performance improvements associated with MIMO control are sensitive to plant modeling errors and the validity range of the linearized model. Indeed, the bandwidth limitation that precludes feedback from being used to reduce the effect of the CAM disturbance upon the A/F loop also prevents feedback from being used to reduce the effects of modeling uncertainty

upon A/F.

VIII. Simulation Example.

In this section simulations of the nonlinear plant with the linear controllers are presented. The simulation in Fig. 15 shows that the simplified multivariable controller results in better A/F control than the decentralized controller even during large throttle steps. Thus, the performance improvements due to the simplified multivariable feedback controller can potentially be realized without elaborate gain scheduling.

Figure 16 illustrates the performance improvements that the VCT engine can achieve when compared to conventional engine (fixed cam phasing). It shows the simulated response of the conventional engine (fixed cam phasing) and the VCT engine to a square wave in commanded throttle at 2000 rpm. The sequence of throttle commands is 9.0 degrees (nominal) to 7.2 degrees to 12.0 degrees and back to 7.2 degrees and then to 9.0 degrees. The corresponding cam phasing set-points are 3 degrees to 10 degrees to 35 degrees (maximum) and back to 3 degrees and then to 10 degrees. The conventional engine scheme has fixed cam at 0 degrees.

The resulting torque response of the VCT engine is kept as responsive as the conventional engine in acceleration. During the abrupt deceleration at the 5th second of the simulation, the torque response of the VCT engine has an abrupt transient behavior which might entail drivability problems. It also indicates that the dash-pot system has to be calibrated taking cam timing into account during rapid tip-outs.

The transient A/F response of the VCT engine is similar to the A/F response of the conventional engine satisfying the equivalent catalytic converter efficiency requirement. Therefore the emission improvement of the VCT engine over the conventional scheme can be demonstrated by the feedgas NO_x and HC emissions. Using the integrated area defined by the NO_x and HC emission curves as a crude measurement of engine emissions, we can estimate a possible reduction of 10% in NO_x and 20% in HC during that period. Moreover, the engine operates at higher manifold pressure, which may reduce the pumping losses and provide an improvement in fuel economy.

IX. Conclusions.

Variable cam timing fundamentally affects both A/F and torque response. To achieve satisfactory performance, the engine controller must take these interactions into account. In this paper we analyze the implication of these interactions in the control design parameters and controller stucture. We formulate the cam timing problem as a set-point tracking problem with closed-loop bandwidth that achieves a reasonable tradeoff between torque performance and averaged feedgas emissions. This bandwidth however, allows high frequency interactions between the cam timing loop and the A/F loop and favors a multivariable feedback controller design.

Fig. 15. Simulation response of the multivariable (MIMO) and the decentralized (2 PI loops) control scheme.

In an effort to achieve efficient controller development for the VCT engine, we investigate the relative utility of a decentralized controller architecture versus a multivariable control strategy. We show that a fully multivariable controller is not necessary. In fact, we simplified the 2x2 multivariable controller by eliminating the cross-coupling term that modifies the cam command based on A/F. On the other hand, we show that allowing the fuel command to depend upon the cam phasing results in smaller A/F transients. The simplified lower triangular controller structure will be used in future work to schedule the linear time-invariant controller over a wide range of engine operation. Finally, nonlinear simulations were used in this paper to demonstrate the potential performance improvements achieved by the variable cam timing engine.

X. Acknowledgment.

The authors wish to thank Jeffrey A. Cook and Kenneth R. Butts of Ford Motor Company, Scientific Research Laboratory for the guidance and constant support throughout this project.

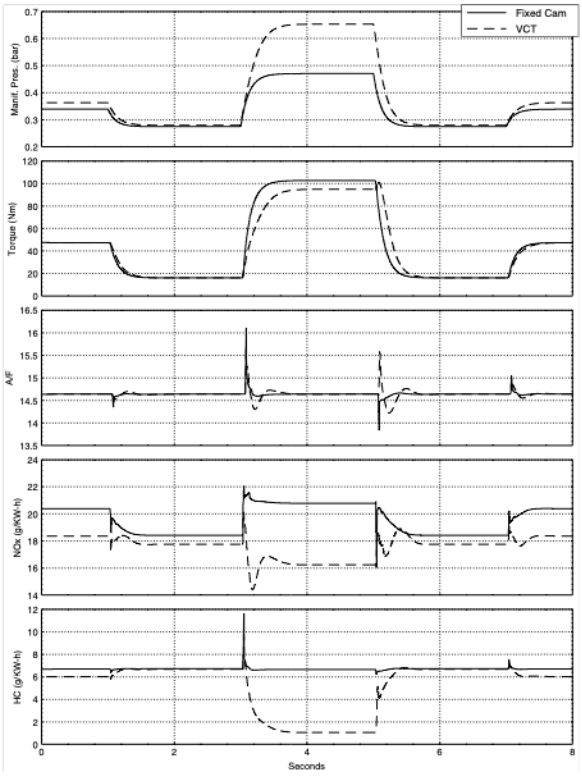

Fig. 16. Simulation response of the conventional ($CAM = 0$) and the VCT engine.

Appendix

I. VCT Engine Model

The low-frequency, phenomenological engine model used for the control development is briefly described here. For the specific functions and values, see [17].

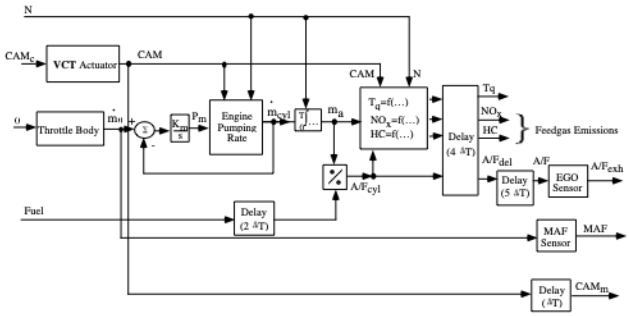

Fig. 17. Block diagram of the VCT engine model.

1. Flow through the Throttle Body

Assumptions: One-dimensional, quasi-steady, compressible flow of an ideal gas.

$$\dot{m}_\theta = g_1(P_m) \cdot g_2(\theta)$$

$$g_1(P_m) = \begin{cases} 1 & \text{if } P_m \le P_O/2 \\ \frac{2}{P_O}\sqrt{P_m P_O - P_m^2} & \text{if } P_m > P_O/2 \end{cases}$$

$$g_2(\theta) = f_1(\theta)$$

2. Inlet Manifold

Assumptions: Ideal gas law, conservation of mass, thermodynamic energy, and momentum, uniform pressure and temperature, constant temperature, no partial pressure due to exhaust gas in the intake manifold at quasi-steady conditions.

$$\frac{d}{dt}P_m = K_m(\dot{m}_\theta - \dot{m}_{cyl}), \text{ where } K_m = \frac{R \cdot T}{V_m} \quad .$$

3. Air Flow into the Cylinders

Assumptions: Low-frequency, quasi-steady representation, uniform flow.

$$\begin{aligned} [\dot{m}_{cyl}] = &\quad f_2(CAM, P_m, N) \\ \dot{m}_{cyl}(t) = &\quad [\dot{m}_{cyl}](t) \quad . \end{aligned}$$

4. Fundamental Sampling Interval

$$\Delta T = \frac{120}{N \cdot n}$$

5. Cylinder Air Charge

$$m_a = \int_0^{\Delta T} \dot{m}_{cyl} dt$$

6. In Cylinder Air-to-Fuel Ratio

$$A/F_{cyl} = \frac{m_a(t)}{F(t - 2\Delta T)}$$

7. Brake Torque

$$\begin{aligned} [T_b] = &\quad f_3(m_a, A/F_{cyl}, N) \\ T_b(t) = &\quad [T_b](t - 4\Delta T) \quad . \end{aligned}$$

8. Feedgas NO_x

$$\begin{aligned} [NO_x] = &\quad f_4(N, CAM, A/F_{cyl}, P_m) \\ NO_x(t) = &\quad [NO_x](t - 6\Delta T) \quad . \end{aligned}$$

9. Feedgas NO_x

$$\begin{aligned} [HC] = &\quad f_5(N, CAM, A/F_{cyl}, P_m) \\ HC(t) = &\quad [HC](t - 6\Delta T) \quad . \end{aligned}$$

10. Camshaft timing phasor+Position Controller

$$\tau_{cam}\frac{d}{dt}CAM_{act}(t) + CAM_{act}(t) = CAM_{com}(t)$$

11. Air-to-Fuel Ratio Measurement

$$(\tau_{exh} + \tau_{ego})\frac{d}{dt}A/F_{exh}(t) + A/F_{exh}(t) = A/F_{cyl}(t - 9\Delta T)$$

12. Mass Air Flow Measurement

$$\tau_{hwa}\frac{d}{dt}MAF(t) + MAF(t) = \dot{m}_\theta(t)$$

13. CAM Measurement

$$CAM_m(t) = CAM_{act}(t - \Delta T)$$

II. Multivariable Controller

The TITO controller was designed to track the desired cam phasing (value from the scheduling map) and maintain A/F at stoichiometry by controlling fuel and cam phasing command using the cam phasing position measurement, the A/F signal from the EGO sensor, and throttle position measurement. We linearized the model at a throttle position equal to 9.33 degrees, cam phasing equal to 10 degrees, and engine speed equal to 2000 rpm. This operating point lies in the transition region on the cam phasing scheduling scheme shown in Fig. 4. The delays are represented by 1st and 2nd order Padé approximations. The linear model has 9 states. The state space representation of the linearized model is given by :

$$\begin{aligned} \dot{x}(t) &= Ax(t) + Bu(t) + B_r r(t) \\ y(t) &= Cx(t) + Du(t) \end{aligned}$$

where

$$\begin{aligned} x &= \begin{bmatrix} P_m \text{ (manifold pressure)} \\ A/F_{exh} \text{ (at the UEGO sensor)} \\ X \text{ (air charge estimator state)} \\ MAF \text{ (mass air flow)} \\ CAM_m \text{ (measured cam phas.)} \\ CAM_a \text{ (actual cam phas.)} \\ F_{del} \text{ (delayed fuel)} \\ A/F \text{ (at the cat. conv.)} \\ A/F_{cyl} \text{ (at the cylinder)} \end{bmatrix}, \\ u &= \begin{bmatrix} CAM_c \text{ (cam phas. command)} \\ F_c \text{ (fuel command)} \end{bmatrix} \\ r &= [\theta \text{ (throttle position)}], \text{ and} \\ y &= \begin{bmatrix} A/F_{exh} \text{ (A/F measurement)} \\ CAM_m \text{ (cam phas. measured)} \end{bmatrix}. \end{aligned}$$

During changes in throttle position, it is important to maintain A/F at stoichiometry and maintain zero tracking error in the cam timing. This is accomplished by augmenting the state vector with the integral of the error in the A/F ($\dot{q}_1 = A/F_{stoic} - A/F_{exh}$), and the integral of the error in the cam timing ($\dot{q}_2 = CAM_{des} - CAM_m$). The augmented input and state vector are:

$$\hat{r} = \begin{bmatrix} \theta \\ A/F_{stoic} \\ CAM_{des} \end{bmatrix} \text{ , and } \hat{x} = \begin{bmatrix} x \\ q \end{bmatrix}.$$

The controller feedback gain $u = -K\hat{x} = \begin{bmatrix} -K_1 & -K_2 \end{bmatrix} \begin{bmatrix} x \\ q \end{bmatrix}$ is found by solving the LQR problem. The weighting matrices R_{xx} and R_{uu} used in the minimization of the cost function $J = \int_0^\infty (\hat{x}' R_{xx} \hat{x} + u' R_{uu} u)\, dt$ are:

$$\begin{aligned} R_{xx} &= diag([0.364,\ 1500,\ 0.3,\ 18,\ 1000,\ 1000,\ 0.9, \\ &\qquad \ldots 1500,\ 1500,\ 70000,\ 5000]) \\ R_{uu} &= diag([1,\ 1]) \end{aligned}$$

The observer gains are derived from a Kalman filter design by minimizing the covariance between the actual and the estimated values of the state. The real symmetric positive semi-definite matrix representing the intensities of the state noises Q_{xx}, and the real symmetric positive definite matrix representing the intensities of the measurement noises Q_{yy} are assumed diagonal. The Kalman filter gain is adjusted so that the LQG controller can asymptotically approach the robustness properties of the LQR design. Loop transfer recovery in the input is employed and the chosen constant values for the covariance matrices Q_{xx}, and Q_{yy} are :

$$\begin{aligned} Q_{xx} &= 0.001 * diag([1, 100, 1, 1000, 100, 100, 0.9, 100, 100]) \\ Q_{yy} &= 100 \cdot diag([1, 1]). \end{aligned}$$

III. Decentralized Controller

The decentralized control design involves defining the two single-input single-output feedback loops that satisfy the design specifications. The transfer function describing the dynamics in the cam phasing loop (p_{11} term) is given by :

$$CAM = \underbrace{\frac{-0.01348(s - 2000)}{s + 26.96}}_{p_{11}(s)} CAM_c \ . \tag{10}$$

The transfer function describing the dynamics in the A/F loop (p_{22} term) is given by :

$$A/F_{exh} = \underbrace{\frac{(s - 133.34)(s^2 - 88.8081s + 2633.67)}{(s + 14.286)(s + 133.33)(s^2 + 88.8081s + 2619.44)}}_{p_{22}(s)} F_c \ . \tag{11}$$

To meet the design specifications on the cam phasing loop the controller was chosen to be :

$$CAM_c = \underbrace{\frac{0.3425(s + 26.96)}{s}}_{c_{11}(s)} CAM_{error} \ . \tag{12}$$

A few design iterations resulted the following controller in the A/F feedback loop :

$$F_c = \underbrace{\frac{0.57(s + 10)}{s}}_{c_{22}(s)} A/F_{error} \ . \tag{13}$$

Both controller designs achieve the bandwidth requirement in the cam phasing loop, and provide adequate speed of response in the A/F loop. The bandwidth specifications for the two loops essentially fix the bandwidths of the diagonal elements of the controller independently of the controller structure. As a result, the diagonal elements of the two controllers are approximately identical (see Fig. 8).

References

[1] E. P. Brandt and J. W. Grizzle, Dynamic Modeling of a Three-Way Catalyst for SI Engine Exhaust Emission Control, to appear in IEEE T-Control Technology.

[2] J. A. Cook, W. J. Johnson, "Automotive Powertrain Control: Emission Regulation to Advanced Onboard Control Systems", Proceedings of the American Control Conference, Seattle, pp. 2571-2575, June 1995.

[3] A. C. Elrod and M. T. Nelson, "Development of a Variable Valve Timing Engine to Eliminate the Pumping Losses Associated with Throttled Operation," SAE Paper No. 860537, 1986.

[4] J. S. Freudenberg, J. W. Grizzle and B. A. Rashap, "A Feedback Limitation of Decentralized Controllers for TITO Systems, with Application to a Reactive Ion Etcher," Proc. 1994 Conference on Decision and Control, pp. 2312-2317, Orlando, 1994.

[5] C. Gray, "A Review of Variable Engine Valve Timing," SAE Paper No. 880386, 1988.

[6] J. W. Grizzle, J. A. Cook and W. P. Milam, "Improved Transient Air-Fuel Ratio Control using Air Charge Estimator," Proc. 1994 Amer. Contr. Conf., Vol. 2, pp. 1568-1572, June 1994.

[7] S. C. Hsieh, A. G. Stefanopoulou, J. S. Freudenberg, and K. R. Butts, " Emission and Drivability Tradeoffs in a Variable Cam Timing SI Engine with Electronic Throttle," Proc. 1997 Amer. Contr. Conf., pp. 284-288, Albuquerque, 1997.

[8] M. Jankovic, F. Frischmuth, A. G. Stefanopoulou, and J. A. Cook, "Torque Management of Engines with Variable Cam Timing," IEEE Control Systems Magazine, vol. 18, pp. 34-42, Oct. 1998.

[9] T. G. Leone, E. J. Christenson, and R. A. Stein, "Comparison of Variable Camshaft Timing Strategies at Part Load," SAE Paper No. 960584, 1996.

[10] T. H. Ma, "Effects of Variable Engine Valve Timing on Fuel Economy," SAE Paper No. 880390, 1988.

[11] J. M. Maciejowski, *Multivariable Feedback Control*, Addison-Wesley Publishing Company, 1989.

[12] G.-B. Meacham, "Variable Cam Timing as an Emission Control Tool," SAE Paper No. 700645, 1970.

[13] M. Morari and E. Zafiriou, *Robust Process Control,* Prentice Hall, 1990.

[14] F. G. Shinskey, *Process Control Systems,* John Wiley & Sons,1989.

[15] M. M. Seron, J. H. Braslavsky, and G. C. Goodwin, *Fundamental Limitations in Filtering and Control*, Springer-Verlag 1997.

[16] A. G. Stefanopoulou and I. Kolmanovsky, "Dynamic Scheduling of Internal Exhaust Gas Recirculation Systems," Proc. IMECE 1997, DSC-Vol. 61, pp. 671-678, Sixth ASME Symposium on Advanced Automotive Technologies, Dallas, 1997.

[17] A. G. Stefanopoulou, J. A. Cook, J. S.Freudenberg, J. W. Grizzle, "Control-Oriented Model of a Dual Equal Variable Cam Timing Spark Ignition Engine," ASME Journal of Dynamic Systems, Measurement and Control, vol. 120, pp. 257-266, 1998.

[18] A. G. Stefanopoulou, J. W. Grizzle and J. S. Freudenberg, "Engine Air-Fuel Ratio and Torque Control using Secondary Throttles," Proc. 1994 Conf. on Decision and Control, pp. 2748-2753, Orlando, 1994.

[19] A. G. Stefanopoulou and I. Kolmanovsky, "Analysis and Control of Transient Torque Response in Engines with Internal Exhaust Gas Recirculation," IEEE Transactions on Control System Technology, to appear.

[20] R. A. Stein, K. M. Galietti and T. G. Leone, "Dual Equal VCT— A Variable Camshaft Timing Strategy for Improved Fuel Economy and Emissions," SAE Paper No. 950975, 1995.

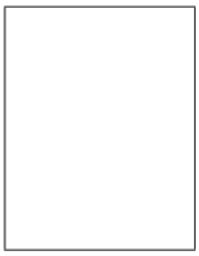

Anna G. Stefanopoulou obtained her Diploma (1991, Nat. Tech. Univ. of Athens, Greece) and M.S. (1992, Univ. of Michigan, U.S.) in Naval Architecture and Marine Engineering. She received her M.S. (1994) and her Ph.D. (1996) in Electrical Engineering and Computer Sc. from the University of Michigan. Dr. Stefanopoulou is presently an Assistant Professor at the Mechanical Engineering Dept. at the University of California, Santa Barbara. Dr. Stefanopoulou is Vice-chair of the Transportation Panel in ASME DSCD and a recipient of a 1997 NSF CAREER award. Her research interests are multivariable feedback theory, control architectures for industrial applications, and powertrain modeling and control.

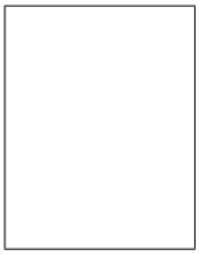

James S. Freudenberg received BS degrees in mathematics and physics from Rose-Hulman Institute of Technology, and the MS and PhD degrees in electrical engineering from the University of Illinois in 1982 and 1985. Since 1984 he has been on the faculty of the University of Michigan, where he is currently an Associate Professor in the Electrical Engineering and Computer Science Department. Dr. Freudenberg received a Presidential Young Investigator Award, and is a past Associate Editor of the IEEE Transactions on Automatic Control. His research interests are in the theory of fundamental design limitations, and in applications to automotive powertrain and semiconductor manufacturing control.

A recent picture of Dr. Freudenberg can be found in the December 1997 issue IEEE Transactions on Automatic Control.

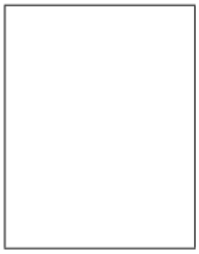

Jessy W. Grizzle received the Ph.D. in electrical engineering from The University of Texas at Austin in 1983. Since September 1987, he has been with The University of Michigan, Ann Arbor, where he is a Professor of Electrical Engineering and Computer Science. He is a past Associate Editor of the Transactions on Automatic Control and Systems & Control Letters, served as Publications Chairman for the 1989 CDC, and in 1997 was elected to the Control Systems Society's Board of Governors. Dr. Grizzle's major research interests lie in the field of control systems. Since his doctoral work, he has investigated theoretical questions in nonlinear systems, where he has concentrated on discrete-time problems and observer design. He has been a consultant in the automotive industry since 1986, where he jointly holds several patents dealing with emissions reduction through improved controller design. In 1992, along with K. L. Dobbins and J. A. Cook of Ford Motor Company, he received the Paper of the Year Award from the IEEE Vehicular Technology Society. Since 1991, he has worked with an interdisciplinary team of researchers at the University of Michigan on applying systems and control techniques to improve the operation of plasma-based microelectronics manufacturing equipment. Dr. Grizzle was a NATO Postdoctoral Fellow from January to December 1984; he received a Presidential Young Investigator Award in 1987, the University of Michigan's Henry Russell Award for outstanding research in 1993, a College of Engineering Teaching Award, also in 1993, and was elected to Fellow of the IEEE in 1997.